AGU100 ADVANCING EARTH AND SPACE SCIENCE

Geophysical Research Letters

RESEARCH LETTER
10.1029/2018GL079936

Key Points:
- When the Moon passes through the geomagnetic tail, a tenuous ionosphere exists at least 50% of the time above the dayside lunar surface
- The day-night asymmetry and dawn-dusk symmetry of the observed ionosphere favors formation by photoionization of a symmetric exosphere
- The lunar-derived plasma density commonly exceeds the ambient density in the tail, allowing lunar plasma to locally perturb the environment

Correspondence to:
J. S. Halekas,
jasper-halekas@uiowa.edu

Citation:
Halekas, J. S., Poppe, A. R., Harada, Y., Bonnell, J. W., Ergun, R. E., & McFadden, J. P. (2018). A tenuous lunar ionosphere in the geomagnetic tail. *Geophysical Research Letters*, *45*. https://doi.org/10.1029/2018GL079936

Received 6 AUG 2018
Accepted 30 AUG 2018
Accepted article online 4 SEP 2018

A Tenuous Lunar Ionosphere in the Geomagnetic Tail

J. S. Halekas[1], A. R. Poppe[2], Y. Harada[3], J. W. Bonnell[2], R. E. Ergun[4], and J. P. McFadden[2]

[1]Department of Physics and Astronomy, University of Iowa, Iowa City, IA, USA, [2]Space Sciences Laboratory, University of California, Berkeley, CA, USA, [3]Department of Geophysics, Kyoto University, Kyoto, Japan, [4]Laboratory of Atmospheric and Space Physics, University of Colorado Boulder, Boulder, CO, USA

Abstract We utilize measurements of electron plasma frequency oscillations made by the two-probe Acceleration, Reconnection, Turbulence, and Electrodynamics of Moon's Interaction with the Sun mission to investigate the charged particle density in the lunar environment as the Moon passes through the Earth's geomagnetic tail. We find that the Moon possesses a tenuous ionosphere with an average density of ~0.1–0.3 cm^{-3}, present at least 50% of the time in the geomagnetic tail, primarily confined to within a few thousand kilometers of the dayside of the Moon. The day-night asymmetry and dawn-dusk symmetry of the observed plasma suggests that photoionization of a neutral exosphere with dawn-dusk symmetry produces the majority of the lunar-derived plasma. The lunar plasma density commonly exceeds the ambient plasma density in the tail, allowing the presence of the lunar ionosphere to appreciably perturb the local plasma environment.

Plain Language Summary Though usually considered an airless body, the Moon actually possesses a very tenuous atmosphere. Ionization of this atmosphere, primarily by sunlight, creates a lunar ionosphere roughly one million times more tenuous than that of the Earth. At most times, this ionosphere does not noticeably affect the surrounding environment. However, when the Moon passes through the near vacuum of the geomagnetic tail of the Earth each lunar month around full Moon, its presence becomes more important. In this unique environment, the lunar-derived charged particle density becomes comparable to the ambient value, and the presence of the lunar ionosphere can appreciably affect its surroundings. We utilize measurements from lunar orbit to investigate the density, structure, and dynamics of the faint lunar ionosphere and its interaction with the local environment of the geomagnetic tail.

1. Introduction

The Moon has a tenuous collisionless exosphere composed of neutral particles derived from the solar wind, micrometeorites, and the lunar subsurface, and liberated from the regolith by charged particle and photon sputtering, micrometeorite impact, and thermal and chemical release (Cook et al., 2013; Sarantos, Killen, et al., 2012; Stern, 1999). Some release processes, including solar wind sputtering (Elphic et al., 1991; Wurz et al., 2007) and micrometeorite impact (Horányi et al., 2015), can produce charged and neutral particles from the surface. Meanwhile, photoionization, charge exchange, and electron impact ionization produce ions and electrons from the exosphere (Huebner & Mukherjee, 2015; Sarantos, Hartle, et al., 2012). The wide range of neutral and charged particle production and ionization processes, each with different spatial and temporal characteristics, leads to time-dependent and asymmetric plasma production around the Moon.

For the majority of each lunation, the Moon lies exposed to the comparatively fast dense solar wind plasma. Here lunar-derived plasma has much lower density than the ambient plasma except in the near-surface photoelectron sheath (which extends only a few meters above the surface). The electromagnetic fields of the ambient plasma can therefore efficiently accelerate lunar charged particles and sweep them downstream. Despite their low density, spacecraft can easily measure the resulting *pickup ions* (Halekas et al., 2015, 2012, 2013; Hilchenbach et al., 1991; Mall et al., 1998; Yokota et al., 2009), thanks to their high energy. However, their presence has little observable effect on the ambient plasma.

Each lunation, the Moon passes through an environment affected by the presence of the Earth, encountering shocked solar wind plasma in the magnetosheath, the tenuous and slowly moving plasma of the geomagnetic tail lobes, and sometimes the variable plasma sheet and plasma sheet boundary layer. Even in the near vacuum of the tail lobes, with many release and ionization mechanisms dramatically reduced, spacecraft have observed ions of lunar origin (Poppe et al., 2012; Tanaka et al., 2009). In this unique environment, the density of lunar-derived plasma can become comparable to or exceed the ambient plasma density (Harada et al.,

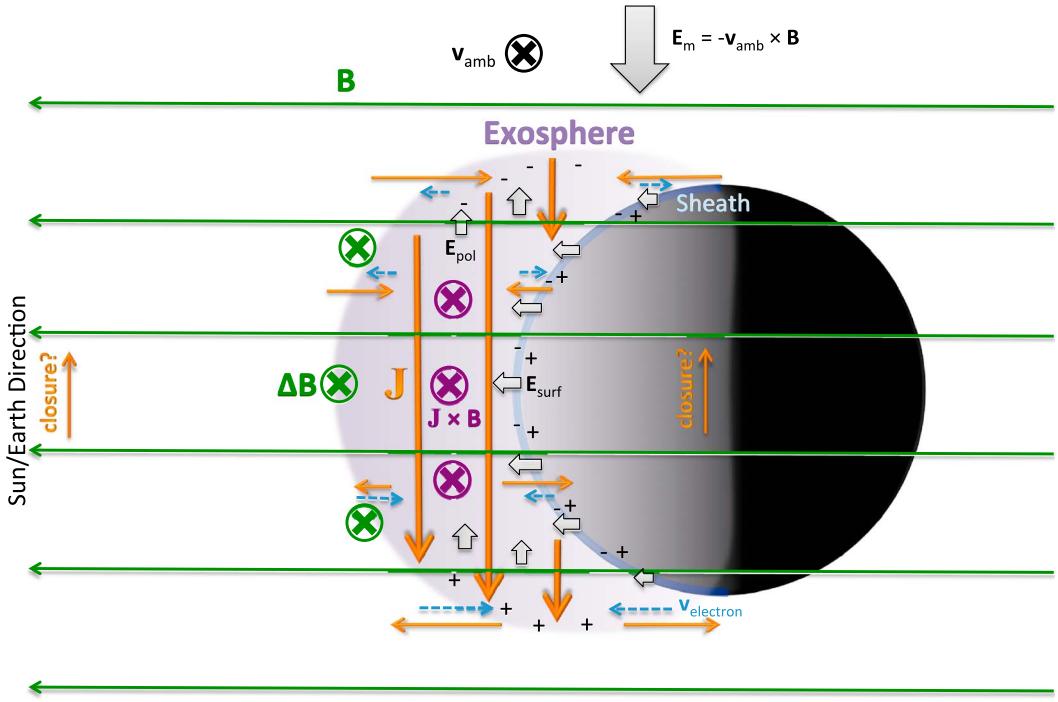

Figure 1. Schematic illustration of the plasma flows, electromagnetic fields, and electric currents around the Moon in the geomagnetic tail.

2013; Poppe et al., 2012; Zhou et al., 2013). Here the presence of lunar plasma can measurably affect the local environment, leading to observable perturbations to electron distributions (Harada et al., 2013) and electric currents (Zhou et al., 2014). Measuring tenuous plasma presents observational difficulties. We now explore the use of plasma wave data to better constrain the plasma density in the lobes.

2. The Lunar Plasma Environment in the Geomagnetic Tail

The interaction of a localized charged particle source with flowing plasma is a well-studied problem from an experimental, observational, and theoretical perspective. The form of the resulting interaction depends on the relative magnitude of the source and ambient plasma densities and pressures, the ratio between the ambient plasma and magnetic field pressures (the plasma β), and the relative flow speed v_{amb} between the ambient plasma and the source.

The Moon in the solar wind provides an example of a plasma release in swiftly flowing $\beta \sim 1$ plasma, with source density much lower than ambient density. In this case, the test particle approximation holds, and lunar charged particles follow simple analytically describable cycloidal trajectories under the influence of the magnetic field and the $-v_{amb} \times$ B motional electric field of the flowing plasma (Halekas et al., 2013; Hartle et al., 2011; Sarantos, Hartle, et al., 2012).

On the other hand, the Moon in the geomagnetic tail provides an example of a plasma release in slowly flowing $\beta \ll 1$ plasma, with source density comparable to or greater than ambient density. In this case, the test particle approximation does not apply, and conservation of momentum requires the ambient plasma to change its velocity appreciably as the plasma source adds mass to the flow, in turn leading to inhomogeneities and driving electric currents. Several analytical/simulation approaches (Chapman & Dunlop, 1986; Sauer et al., 1994; Winske, 1985) can describe this mass loading process (Szego et al., 2000).

Figure 1 illustrates the fields and currents predicted around the Moon in the geomagnetic tail, based on scenarios with comparable parameters such as active experiments by Combined Release and Radiation Effects Satellite (Reasoner, 1992) and the interaction of the inner moons of giant planets with corotating plasma (X. Jia, Kivelson, et al., 2010; Kivelson et al., 2004). In this regime, the source plasma, rather than accommodating immediately to the ambient flow, *skids* before fully coupling to the ambient plasma (Huba

et al., 1992). This initial decoupling results in part from polarization of the source plasma, which creates an electric field E_{pol} that opposes the motional electric field E_m of the ambient plasma. Mass loading locally slows the flow near the source, resulting in a bending of the magnetic field embedded in the plasma (ΔB), driving currents (J) across the source, and producing a J $\times$ B magnetic tension force that acts on the source plasma (Vasylunias, 2016). The resulting structure, known as an Alfvén wing (Drell et al., 1965), extracts momentum from the ambient plasma along an extended region to accelerate the source plasma. The electric current across the source plasma closes, typically primarily along the magnetic field, carried by electron flows ($v_{electron}$). However, parallel electric fields may further decouple the source plasma and complicate the structure of the interaction (Delamere et al., 2000).

The Moon's interaction with the geomagnetic tail has unique aspects due to the presence of a solid insulating obstacle, in contrast to active releases that have no macroscopic obstacle or outer planet moons that have more significant ionospheric and/or subsurface conductivity. Y.-D. Jia, Russell, et al. (2010) simulated plasma flow onto a mass loading region centered on an absorbing body but for a lower ratio of source to ambient density. They did not incorporate the effects of charge accumulation on the surface from photoemission and the resulting outward electric fields E_{surf} in the near-surface plasma sheath (shown in Figure 1), which add another source of acceleration at low altitudes and perturb the trajectories of ions around the Moon (Poppe et al., 2013). These near-surface fields may also affect the closure of mass loading currents and alter the electromagnetic structure of the interaction. Parallel currents and/or electric fields may lead to the observed perturbations to electron distributions (Harada et al., 2013).

A continuity equation of the form $\frac{\partial n}{\partial t} = Q - \nabla\cdot\left(n\,\vec{v}\right)$ should govern the dynamics of the plasma around the Moon, with n, v, and Q representing the local plasma density, flow velocity, and production rate. In equilibrium, transport away from the Moon should balance plasma production (recombination is negligible at low densities). Given that plasma can move both along and transverse to the magnetic field, the local density observed near the Moon likely depends sensitively on the source production rate Q and the transverse plasma flow (Daily et al., 1977). For low production rates and/or high flow speeds, lateral transport should rapidly convect plasma away from the Moon, resulting in lower density near the Moon. On the other hand, for high production rates and/or low flow speeds, diffusion along the magnetic field (possibly aided by acceleration in the near-surface sheath) may dominate, leading to denser plasma extending sunward along magnetic field lines from the surface. Modern simulations constrained by observations could potentially differentiate between these scenarios.

3. Lunar Ionosphere Observations

To investigate the lunar environment in the geomagnetic tail, we utilize data from the two-probe Acceleration, Reconnection, Turbulence, and Electrodynamics of Moon's Interaction with the Sun (ARTEMIS) mission (Angelopoulos, 2010), focusing primarily on measurements from the electrostatic analyzer (ESA; McFadden et al., 2008) and Electric Field Instrument (EFI; Bonnell et al., 2008). The ARTEMIS probes occupy elliptical near-equatorial orbits around the Moon, providing two-point observations from a variety of distances and local times, over a long time range extending from late 2011 to the present.

In Figure 2, we show sample observations from the two probes in the geomagnetic tail, during a time period with both tail lobe and plasma sheet/plasma sheet boundary layer encounters (with the latter identifiable by the higher charged particle fluxes). The two probes observe the same structures except when their orbits approach the lunar dayside, where the ESAs observe tenuous additional ion populations and a reduction in energetic electron flux due to absorption of incident electrons by the solid obstacle.

Lunar plasma creates a detectable signature in the density moments computed from both electron and ion distributions, though more clearly so for electrons. The smaller increase in the ion density moment in part reflects the limitations of the moment computation, which assumes all ions are protons, not accounting for the presence of heavy lunar ions (Zhou et al., 2013). In addition, the spacecraft has a large positive electrostatic potential in the tail, which prevents the measurement of low-energy ions and leads to further underestimation of the density. The ion density moments also have an effective *floor* from background counts caused by energetic cosmic rays and natural radioactivity in the microchannel plate detectors, comparable to real counts in low-density regimes. The electron density moments, on the other hand, though they more clearly

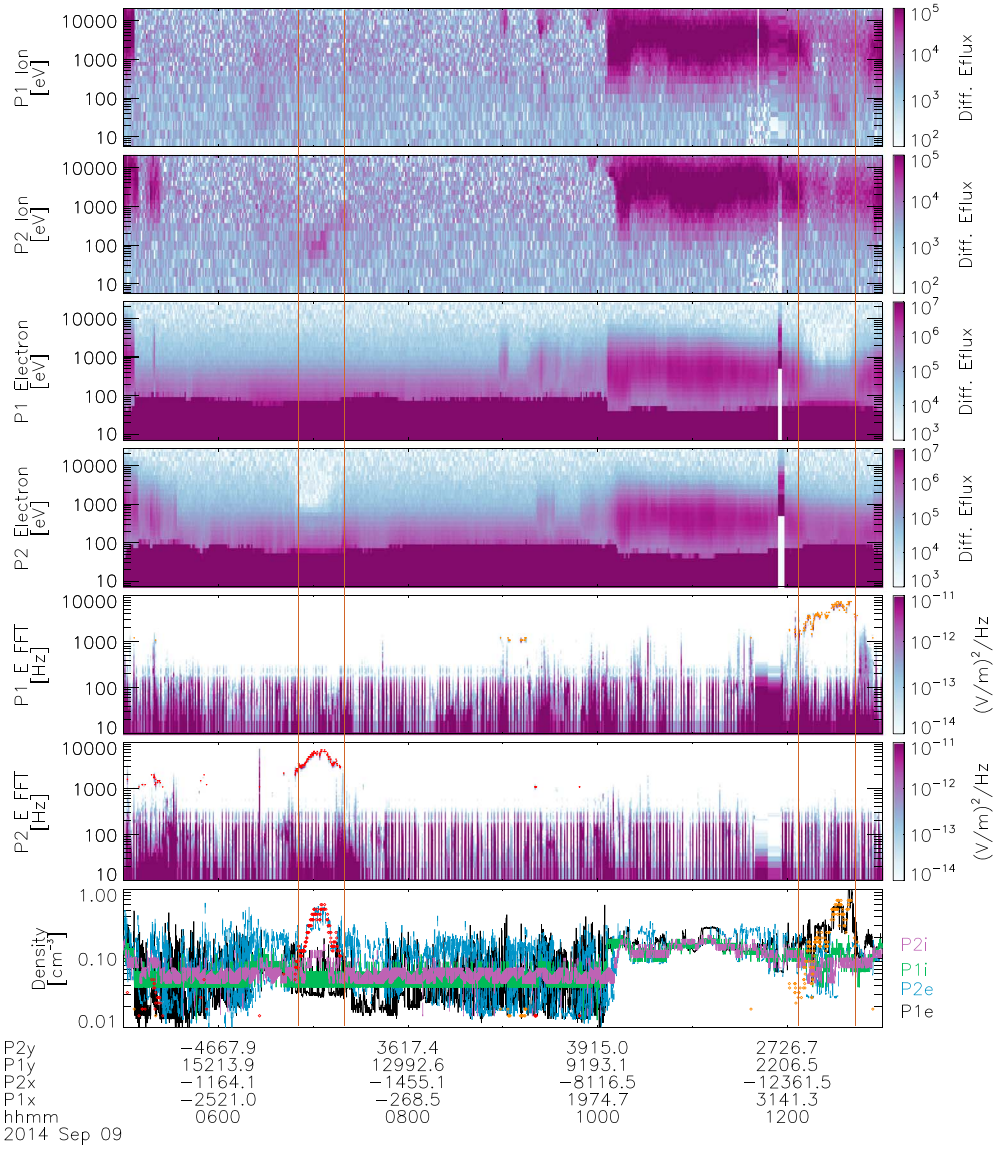

Figure 2. Acceleration, Reconnection, Turbulence, and Electrodynamics of Moon's Interaction with the Sun probe 1 and 2 (P1/P2) measurements in the geomagnetic tail of ion and electron energy spectra (eV/[eV·cm^2·s·sr]), electric field power spectra (Fast Fourier Transforms), and plasma density estimated from ion and electron moment computations and electron plasma frequency oscillations. Red and orange diamonds show plasma frequency values from the fitting and selection process described in the text. Labels indicate probe positions in selenocentric solar ecliptic coordinates and universal time. Orange vertical lines bracket times when probe orbits pass above the dayside surface.

reveal the presence of lunar plasma, become noisy at low densities. This *noise* arises from the need to subtract a high-flux population of spacecraft-generated photoelectrons at lower energies, a separation that the limited ESA energy resolution makes difficult to perform precisely. Therefore, neither ion nor electron moments provide an ideal means to survey the plasma density in a tenuous environment such as the tail lobes.

The alternating current electric field measurements made by the EFI provide an alternative means of investigating the plasma near the Moon. As seen in Figure 2, sporadic narrowband features at 1–10 kHz exist in the electric field spectra observed by the EFI. These represent plasma oscillations at the electron plasma frequency $f_p = \omega_{pe}/(2\pi)$, which we can convert to an estimate of the local plasma density using the relation $n = m_e\varepsilon_0\omega_{pe}^2/e^2$ (note that the difference between the upper hybrid and plasma frequencies is at most a few percent for the parameter regime in question, so we need not distinguish the two). The EFI frequency range (0- to 8-kHz Nyquist) enables measurement of charge densities up to ~0.8 cm^{-3}, adequate to cover

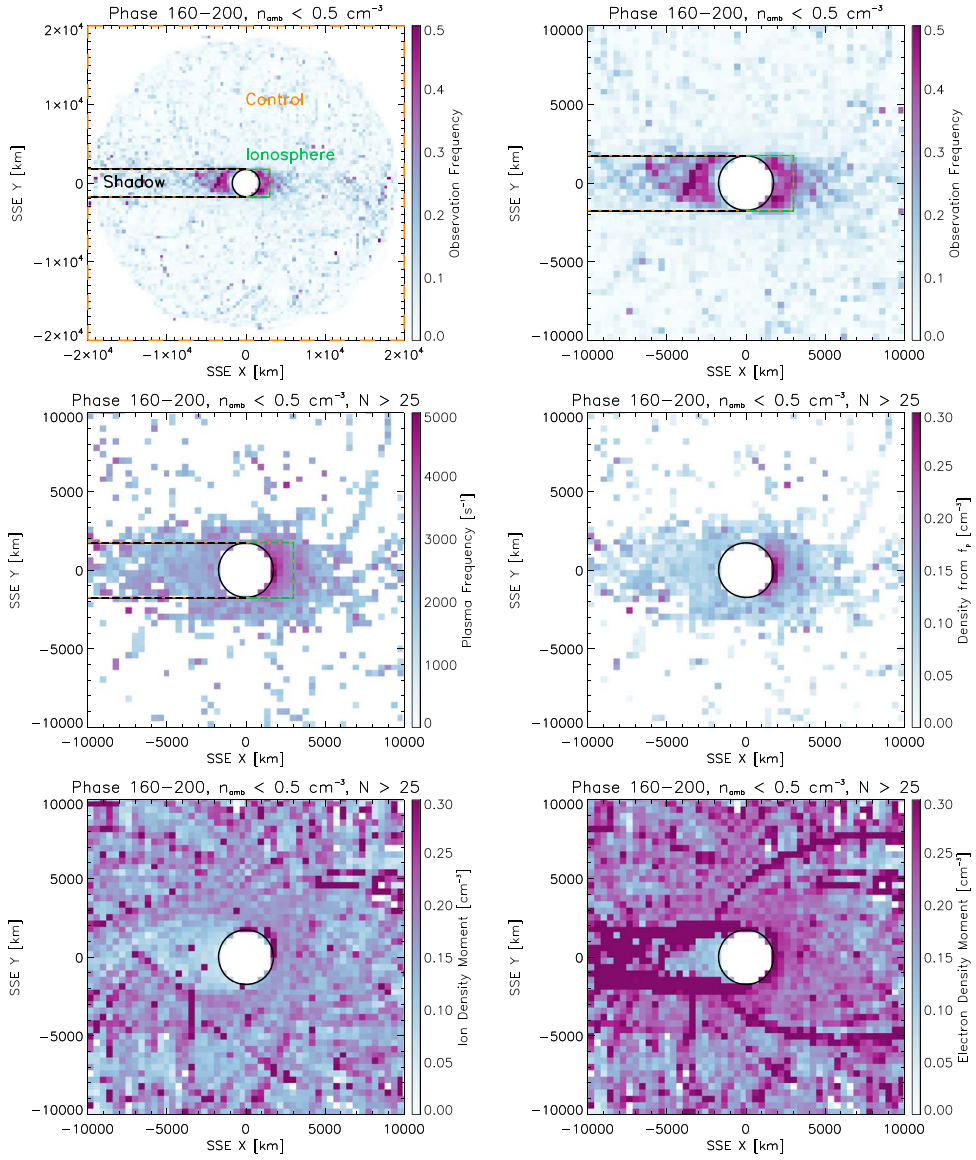

Figure 3. Acceleration, Reconnection, Turbulence, and Electrodynamics of Moon's Interaction with the Sun observations around the Moon in the geomagnetic tail, including the plasma line observation frequency at two spatial scales, the average electron plasma frequency f_p retrieved from Electric Field Instrument measurements, the average plasma density determined from f_p, and the average ion and electron density moments computed from electrostatic analyzer measurements. Orange and green lines outline the dayside *Ionosphere* and the *Control* regions used in the subsequent analysis.

the range typically observed in the tail. The EFI measurements agree with the ESA electron moments for moderate densities but provide much more accurate measurements of plasma densities below ~0.2–0.3 cm^{-3}.

We identify the plasma frequency line by fitting each observed electric field power spectrum (for frequencies greater than 500 Hz, avoiding lower-frequency noise due to probe-shadowing and other sources) to a five-parameter model consisting of a constant plus a linear term plus a Gaussian function. We discard as unreliable fits for which the inferred plasma frequency lies below 1 kHz, the standard deviation of the Gaussian exceeds 15% of the center value, the amplitude of the Gaussian lies below 10^{-13} $(V/m)^2/Hz$, or the standard error of the fit exceeds 30% of the amplitude. Figure 2 includes sample results from this fitting and selection process. We commonly identify the plasma frequency near the Moon but typically only observe it for sporadic intervals at larger distances. This reflects the fact that some type of nonequilibrium electron distribution must generate plasma line oscillations. When ambient and/or lunar plasma is present, the presence of loss cones and/or beams on magnetic field lines that intersect the lunar surface reliably generates plasma oscillations.

We repeat the analysis described above for all EFI measurements from both ARTEMIS probes made from 29 October 2011 to 25 April 2018. We also compute ESA density and velocity moments for the same time period. In order to focus only on low-density environments where EFI can measure the plasma frequency, we restrict our study to lunar phase angles from 160 to 200° (180° = full Moon) and times where the ion density moment from the probe farther from the Moon does not exceed 0.5 cm^{-3}. We show the results of this analysis in Figure 3. As expected given the prevailing magnetic field geometry in the tail, the highest probability of detecting plasma oscillations occurs in a region extending sunward and antisunward from the Moon, with rates of detection up to ~50% within a few lunar radii above both the day and night sides. Outside of this region, rates of plasma line detection rarely exceed a few percent.

Within the region of frequent detection, the average plasma frequency and the density derived from it have clear systematic variations. We find much higher plasma densities above the dayside, with the largest densities at the lowest altitudes, consistent with plasma production by photoionization of an exospheric source. Given the less than 100% detection rate, we can obtain only an incomplete and potentially biased view of the lunar plasma. However, we find that the highest plasma densities occur not in the region with the highest detection rate but at lower altitudes, consistent with the spatial structure expected for an exospheric source. Furthermore, despite roughly equal rates of detection, we find a very clear day-night asymmetry in the value of the plasma density, as expected given the dominant role of photoionization in plasma production in the low-density geomagnetic tail.

To check the results from EFI, we also show the average density from ion and electron moments in Figure 3. Consistent with the observations of Figure 2, we find a clear signature of lunar plasma in the electron moments, with an average density and spatial structure in close agreement with that derived from the plasma frequency; however, the high level of noise in the electron moments in low-density environments obscures the lunar signal. Furthermore, we observe artifacts in and near the shadow region, which result from changes in the spacecraft potential that occur as the EFI changes its biasing scheme before/after shadow periods (note that the probe bias does not affect the alternating current electric field measurements we use to identify the plasma frequency). Meanwhile, the ion moments reveal only a faint signal of lunar plasma, suggesting that most lunar ions lie at energies below the effective detection threshold in the tail. Despite these confounding effects, the ion and electron density moments are not obviously inconsistent with the observed plasma frequency.

We find no obvious evidence of a dense dust-related ionosphere (Imamura et al., 2012) at low altitudes. The observed plasma density appears symmetric between dusk and dawn, which seemingly disfavors a major contribution from micrometeoritic or thermal sources, since both mechanisms should produce higher neutral densities at dawn (Szalay & Horányi, 2015). This is surprising, given the major role for micrometeoritic impact indicated by the Lunar Atmosphere and Dust Environment Explorer mission (Colaprete et al., 2015). Instead, the ARTEMIS observations appear more consistent with photoionization of a symmetric neutral exosphere such as that produced by photon sputtering (photon-stimulated desorption; McGrath et al., 1986). On the other hand, the effects of transport may obscure asymmetries in production rate.

4. Lunar Ionosphere Variability

We next investigate the variability of the lunar plasma density in the geomagnetic tail. This variability should reflect not only the spatial and temporal variability of the exosphere itself (which may depend on micrometeoritic flux [Colaprete et al., 2015], plasma properties [Sarantos et al., 2008; Wilson et al., 2006], and solar photon flux) but also variability in plasma production (primarily dependent on solar ionizing photon flux) and/or plasma transport, as discussed above in section 2. It may also reflect the variability of conditions that favor the observation of plasma oscillations. In Figure 4, we compare the relative probability distributions of retrieved densities derived from the plasma frequency measured in the *Ionosphere* region to those from the *Control* region, for the same data shown in Figure 3.

During time periods with ambient plasma densities in the bottom quartile of our sample ($n_{amb} < 0.06$ cm^{-3}), we find a much higher probability of observing total plasma densities greater than ~0.05 cm^{-3} near the Moon than in our control region, reflecting the dominance of lunar plasma at these times. On the other hand, during time periods with ambient densities in the top quartile ($n_{amb} > 0.17$ cm^{-3}), the probability of

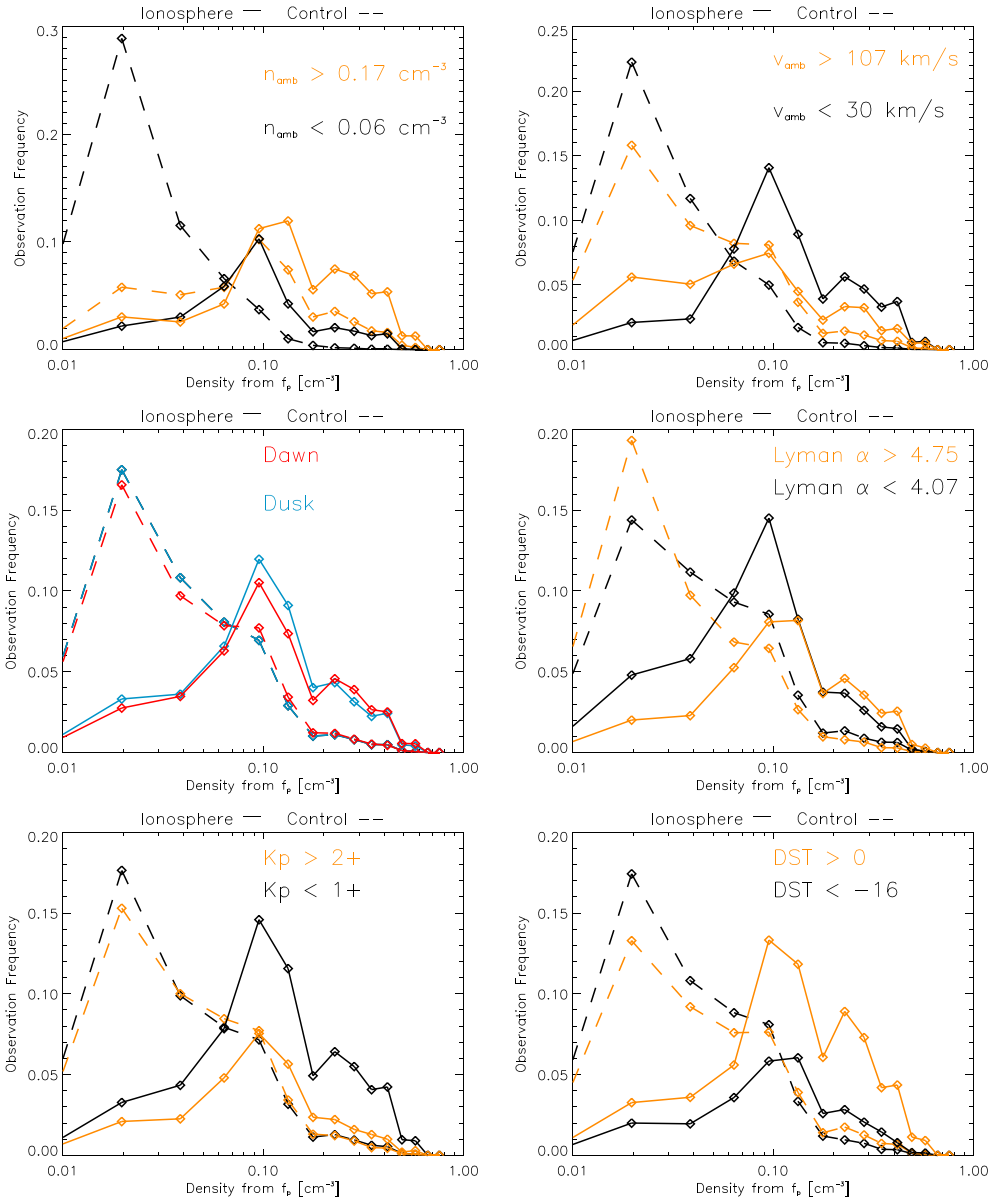

Figure 4. Probability distributions of total plasma densities retrieved from plasma frequency detections by the two Acceleration, Reconnection, Turbulence, and Electrodynamics of Moon's Interaction with the Sun probes in the geomagnetic tail in the *Ionosphere* and *Control* regions defined in Figure 3, for different ranges of ambient plasma density and flow speed (estimated from electrostatic analyzer ion moments), local times, and solar and magnetospheric activity indices. We normalize the distributions so that the two histograms for the ionosphere sample and the two histograms for the control sample independently sum to unity in each panel.

observing a given density near the Moon does not differ as greatly from that in the control region, since the ambient density comprises a greater fraction of the total. The average total density observed near the Moon increases by ~55% from times in the bottom quartile to times in the top quartile, providing a first-order estimate of the contribution of the ambient plasma to the total density. Note that the total density estimated from the plasma frequency does not necessarily exceed the ambient density derived from ion moments, because of the background contribution to the ion moments.

The probability of detecting the plasma frequency near the Moon increases significantly for large ambient densities, with a ~95% higher chance of observing the plasma line for times in the top quartile. This indicates that higher ambient density (and thus higher total density) leads to more favorable conditions for generating

observable plasma frequency oscillations near the Moon, possibly suggesting a minimum total density threshold for detecting lunar plasma. If correct, times with no detections may indicate a lack of appreciable ambient or lunar plasma density near the Moon.

The probability of detecting the plasma frequency near the Moon also increases for lower ambient plasma flow speeds, with a ~37% higher chance of observing the plasma line at times with flow speeds in the bottom quartile, and a ~30% higher average total density for those detections. While we do not consider the flow speed derived from ion moments completely reliable, given the background and energy threshold issues, to first order this supports our conjecture that during periods with high flow speeds we should observe lower (or no) lunar plasma density, since faster convection efficiently transports lunar plasma away from the Moon.

Higher Lyman α flux decreases the probability of detecting the plasma frequency near the Moon by ~23% but increases the average total density for those detections by ~40%. To the extent that Lyman α provides a useful proxy for other solar ultraviolet wavelengths, the increase in total inferred density could reflect an increase in plasma production by photoionization, but the decrease in detection frequency has no obvious explanation.

We find no statistically significant difference in the probability of detecting the plasma frequency near the Moon or in the density retrieved from those detections, between the dawn and dusk hemispheres of the Moon. This confirms the result from the spatial mapping shown in Figure 3 and disfavors a major contribution from asymmetric plasma production mechanisms.

Lower magnetospheric activity (smaller Kp and more positive Dst) dramatically increases the probability of detecting the plasma frequency near the Moon, with a ~120% higher chance of observing the plasma line during the bottom quartile of magnetospheric activity and a ~20% higher average total density for those detections. This result also may support our conjecture regarding the role of transport in regulating the local plasma density near the Moon.

It remains unclear to what degree the variations in plasma density that we observe near the Moon reflect variations in exospheric neutral density. Previous studies have suggested that the neutral density for some exospheric species may increase in the plasma sheet (Sarantos et al., 2008; Wilson et al., 2006). Our results suggest that the higher ambient density in the plasma sheet would not significantly increase the lunar plasma density, and the higher flow speeds in and near the plasma sheet might even decrease the lunar plasma density. However, given the significant role of transport in regulating the local plasma density, we cannot necessarily infer similar systematics for the neutral density.

5. Conclusions

The lunar environment in the geomagnetic tail provides an intriguing area of study, with broad relevance to surface-bounded exospheres throughout our solar system and beyond, and to our understanding of the fundamental physics of plasma releases in tenuous environments. The presence of lunar-derived plasma in the geomagnetic tail may also have relevance for the coupling between the Moon and the Earth. Charged particles can travel from the Moon to the near-Earth environment (Halekas et al., 2011) and may thus affect the environment not only near the Moon but also where magnetic field lines connect the Moon to the Earth's ionosphere. Conversely, plasma observed near the Moon may include not only lunar-derived material but also material derived from the terrestrial ionosphere (Poppe et al., 2016).

Although many aspects of the unique lunar environment in the geomagnetic tail remain challenging to measure and interpret, the ARTEMIS EFI plasma frequency oscillation measurements discussed in this paper provide new constraints on the lunar exosphere and its interaction with the tenuous plasma in the geomagnetic tail. These measurements demonstrate that 50% or more of the time, a tenuous collisionless ionosphere populated by lunar-derived plasma exists above the dayside of the Moon as it passes through the geomagnetic tail. The density, spatial distribution, and variability of this plasma all provide valuable constraints on the sources, sinks, composition, and structure of the lunar exosphere, and upon the nature of the interaction between lunar-derived plasma and the geomagnetic environment. Developing a detailed understanding of the physics of this unique scenario will require a more thorough theoretical treatment and likely detailed multidimensional plasma simulations. This observational investigation provides a starting point for these future studies.

Acknowledgments
We acknowledge support from NASA grant NNX15AP89G, the SSERVI DREAM2 team, and the THEMIS contract NAS5–02099. All ARTEMIS data are publicly available at NASA's CDAWeb (https://cdaweb.sci.gsfc.nasa.gov) and the ARTEMIS site (http://artemis.ssl.berkeley.edu). We acknowledge Jim King and Natalia Papitashvili for activity indices used in the study, provided through OmniWeb (https://omniweb.gsfc.nasa.gov).

References

Angelopoulos, V. (2010). The ARTEMIS mission. *Space Science Reviews*, *165*(1-4), 3–25. https://doi.org/10.1007/s11214-010-9687-2

Bonnell, J. W., Mozer, F. S., Delory, G. T., Hull, A. J., Ergun, R. E., Cully, C. M., et al. (2008). The electric field instrument (EFI) for THEMIS. *Space Science Reviews*, *141*, 303–341.

Chapman, S. C., & Dunlop, M. W. (1986). Ordering of momentum transfer along VvB in the AMPTE solar wind releases. *Journal of Geophysical Research*, *91*(A7), 8051–8055. https://doi.org/10.1029/JA091iA07p08051

Colaprete, A., Sarantos, M., Wooden, D. H., Stubbs, T. J., Cook, A. M., & Shirley, M. (2015). How surface composition and meteoroid impacts mediate sodium and potassium in the lunar exosphere. *Science*, *351*(6270), 249–252. https://doi.org/10.1126/science.aad2380

Cook, J. C., Stern, S. A., Feldman, P. D., Gladstone, G. R., Retherford, K. D., & Tsang, C. C. C. (2013). New upper limits on numerous atmospheric species in the native lunar atmosphere. *Icarus*, *225*(1), 681–687. https://doi.org/10.1016/j.icarus.2013.04.010

Daily, W. D., Barker, W. A., Clark, M., Dyal, P., & Parkin, C. W. (1977). Ionosphere and atmosphere of the Moon in the geomagnetic tail. *Journal of Geophysical Research*, *82*(33), 5441–5451. https://doi.org/10.1029/JB082i033p05441

Delamere, P. A., Stenbaek-Nielsen, H. C., Swift, D. W., & Otto, A. (2000). Momentum transfer in the combined release and radiation effects satellite plasma experiments: The role of parallel electric fields. *Physics of Plasmas*, *7*(9), 3771–3780. https://doi.org/10.1063/1.1287741

Drell, S. D., Foley, H. M., & Ruderman, M. A. (1965). Drag and propulsion of large satellites in the ionosphere: An Alfvén propulsion engine in space. *Journal of Geophysical Research*, *70*(13), 3131–3145. https://doi.org/10.1029/JZ070i013p03131

Elphic, R. C., Funsten, H. O., Barraclough, B. L., McComas, D. J., Paffett, M. T., Vaniman, D. T., & Heiken, G. (1991). Lunar surface composition and solar wind-induced secondary ion mass spectrometry. *Geophysical Research Letters*, *18*(11), 2165–2168. https://doi.org/10.1029/91GL02669

Halekas, J. S., Benna, M., Mahaffy, P. R., Elphic, R. C., Poppe, A. R., & Delory, G. T. (2015). Detections of lunar exospheric ions by the LADEE neutral mass spectrometer. *Geophysical Research Letters*, *42*, 5162–5169. https://doi.org/10.1002/2015GL064746

Halekas, J. S., Delory, G. T., Farrell, W. M., Angelopoulos, V., McFadden, J. P., Bonnell, J. W., et al. (2011). First remote measurements of lunar surface charging from ARTEMIS: Evidence for nonmonotonic sheath potentials above the dayside surface. *Journal of Geophysical Research*, *116*, A07103. https://doi.org/10.1029/2011JA016542

Halekas, J. S., Poppe, A. R., Delory, G. T., Sarantos, M., Farrell, W. M., Angelopoulos, V., & McFadden, J. P. (2012). Lunar pickup ions observed by ARTEMIS: Spatial and temporal distribution and constraints on species and source locations. *Journal of Geophysical Research*, *117*, E06006. https://doi.org/10.1029/2012JE004107

Halekas, J. S., Poppe, A. R., Delory, G. T., Sarantos, M., & McFadden, J. P. (2013). Using ARTEMIS pickup ion observations to place constraints on the lunar atmosphere. *Journal of Geophysical Research: Planets*, *118*, 81–88. https://doi.org/10.1029/2012JE004292

Harada, Y., Machida, S., Halekas, J. S., Poppe, A. R., & McFadden, J. P. (2013). ARTEMIS observations of lunar dayside plasma in the terrestrial magnetotail lobe. *Journal of Geophysical Research: Space Physics*, *118*, 3042–3054. https://doi.org/10.1002/jgra.50296

Hartle, R. E., Sarantos, M., & Sittler, E. C. Jr. (2011). Pickup ion distributions from three-dimensional neutral exospheres. *Journal of Geophysical Research*, *116*, A10101. https://doi.org/10.1029/2011JA016859

Hilchenbach, M., Hovestadt, D., Klecker, B., & Mobius, E. (1991). Detection of singly ionized energetic lunar pick-up ions upstream of Earth's bow shock. In E. Marsch & G. Schwenn (Eds.), *Solar wind seven* (pp. 150–155). New York: Pergamon.

Horányi, M., Szalay, J. R., Kempf, S., Schmidt, J., Grün, E., Srama, R., & Sternovsky, Z. (2015). A permanent asymmetric dust cloud around the moon. *Nature*, *522*(7556), 324–326. https://doi.org/10.1038/nature14479

Huba, J. D., Mitchell, H. G., Fedder, J. A., & Bernhardt, P. A. (1992). 'Skidding' of the CRRES G-9 barium release. *Geophysical Research Letters*, *19*(11), 1085–1088. https://doi.org/10.1029/92GL01109

Huebner, W. F., & Mukherjee, J. (2015). Photoionization and dissociation rates in solar and blackbody radiation fields. *Planetary and Space Science*, *106*, 11–45. https://doi.org/10.1016/j.pss.2014.11.022

Imamura, T., Nabatov, A., Mochizuki, N., Iwata, T., Hanada, H., Matsumoto, K., et al. (2012). Radio occultation measurement of the electron density near the lunar surface using a subsatellite on the SELENE mission. *Journal of Geophysical Research*, *117*, A06303. https://doi.org/10.1029/2011JA017293

Jia, X., Kivelson, M. G., Khurana, K. K., & Walker, R. J. (2010). Magnetic fields of the satellites of Jupiter and Saturn. *Space Science Reviews*, *152*(1-4), 271–305. https://doi.org/10.1007/s11214-009-9507-8

Jia, Y.-D., Russell, C. T., Khurana, K. K., Toth, G., Leisner, J. S., & Gombosi, T. I. (2010). Interaction of Saturn's magnetosphere and its moons: 1. Interaction between corotating plasma and standard obstacles. *Journal of Geophysical Research*, *115*, A04214. https://doi.org/10.1029/2009JA014630

Kivelson, M. G., Bagenal, F., Kurth, W. S., Neubauger, F. M., Paranicas, C., & Saur, J. (2004). Magnetospheric interactions with satellites. In B. F. Bagenal, T. E. Dowling, & W. B. McKinnon (Eds.), *Jupiter: The planet, satellites and magnetosphere* (pp. 513–536). Cambridge: Cambridge University Press.

Mall, U., Kirsch, E., Cierpka, K., Wilken, B., Soding, A., Neubauer, F., et al. (1998). Direct observation of lunar pick-up ions near the Moon. *Geophysical Research Letters*, *25*(20), 3799–3802. https://doi.org/10.1029/1998GL900003

McFadden, J. P., Carlson, C. W., Larson, D., Ludlam, M., Abiad, R., Elliott, B., et al. (2008). The THEMIS ESA plasma instrument and in-flight calibration. *Space Science Reviews*, *141*, 277–302.

McGrath, M. A., Johnson, R. E., & Lanzerotti, L. J. (1986). Sputtering of sodium on the planet mercury. *Nature*, *323*(6090), 694–696. https://doi.org/10.1038/323694a0

Poppe, A. R., Fillingim, M. O., Halekas, J. S., Raeder, J., & Angelopoulos, V. (2016). ARTEMIS observations of terrestrial ionospheric molecular ion outflow at the Moon. *Geophysical Research Letters*, *43*, 6749–6758. https://doi.org/10.1002/2016GL069715

Poppe, A. R., Halekas, J. S., Samad, R., Sarantos, M., & Delory, G. T. (2013). Model-based constraints on the lunar exosphere derived from ARTEMIS pickup ion observations in the terrestrial magnetotail. *Journal of Geophysical Research: Planets*, *118*, 1135–1147. https://doi.org/10.1002/jgre.20090

Poppe, A. R., Samad, R., Halekas, J. S., Sarantos, M., Delory, G. T., Farrell, W. M., et al. (2012). ARTEMIS observations of lunar pickup ions in the terrestrial magnetotail lobes. *Geophysical Research Letters*, *39*, L17104. https://doi.org/10.1029/2012GL052909

Reasoner, D. (1992). Chemical-release mission of CRRES. *Journal of Spacecraft and Rockets*, *29*(4), 580–584. https://doi.org/10.2514/3.25502

Sarantos, M., Hartle, R. E., Killen, R. M., Saito, Y., Slavin, J. A., & Glocer, A. (2012). Flux estimates of ions from the lunar exosphere. *Geophysical Research Letters*, *39*, 13101. https://doi.org/10.1029/2012GL052001

Sarantos, M., Killen, R. M., Glenar, D. A., Benna, M., & Stubbs, T. J. (2012). Metallic species, oxygen and silicon in the lunar exosphere: Upper limits and prospects for LADEE measurements. *Journal of Geophysical Research*, *117*, A03103. https://doi.org/10.1029/2011JA010744

Sarantos, M., Killen, R. M., Sharma, A. S., & Slavin, J. A. (2008). Influence of plasma ions on source rates for the lunar exosphere during passage through the Earth's magnetosphere. *Geophysical Research Letters*, *35*, L04105. https://doi.org/10.1029/2007GL032310

Sauer, K., Bogdanov, A., & Baumgärtel, K. (1994). Evidence of an ion composition boundary (protonopause) in bi-ion fluid simulations of solar wind mass loading. *Geophysical Research Letters*, *21*(20), 2255–2258. https://doi.org/10.1029/94GL01691

Stern, S. A. (1999). The lunar atmosphere: History, status, current problems, and context. *Reviews of Geophysics*, *37*(4), 453–491. https://doi.org/10.1029/1999RG900005

Szalay, J. R., & Horányi, M. (2015). Annual variation and synodic modulation of the sporadic meteoroid flux to the moon. *Geophysical Research Letters*, *42*, 10,580–10,584. https://doi.org/10.1002/2015GL066908

Szego, K., Glassmeier, K.-H., Bingham, R., Bogdanov, A., Fischer, C., Haerendel, G., et al. (2000). Physics of mass loaded plasmas. *Space Science Reviews*, *94*, 429–671.

Tanaka, T., Saito, Y., Yokota, S., Asamura, K., Nishino, M. N., Tsunakawa, H., et al. (2009). First in situ observation of the moon-originating ions in the Earth's magnetosphere by MAP-PACE on SELENE (KAGUYA). *Geophysical Research Letters*, *36*, L22106. https://doi.org/10.1029/2009GL040682

Vasylunias, V. M. (2016). Physical origin of pickup currents. *Annales de Geophysique*, *34*(1), 153–156. https://doi.org/10.5194/angeo-34-153-2016

Wilson, J. K., Mendillo, M., & Spence, H. E. (2006). Magnetospheric influence on the Moon's exosphere. *Journal of Geophysical Research*, *111*, A07207. https://doi.org/10.1029/2005JA011364

Winske, D. (1985). Hybrid simulation codes with application to shocks and upstream waves. *Space Science Reviews*, *42*, 53–66.

Wurz, P., Rohner, U., Whitby, J. A., Kolb, C., Lammer, H., Dobnikar, P., & Martín-Fernández, J. A. (2007). The lunar exosphere: The sputtering contribution. *Icarus*, *191*(2), 486–496. https://doi.org/10.1016/j.icarus.2007.04.034

Yokota, S., Saito, Y., Asamura, K., Tanaka, T., Nishino, M. N., Tsunakawa, H., et al. (2009). First direct detection of ions originating from the Moon by MAP-PACE IMA onboard SELENE (KAGUYA). *Geophysical Research Letters*, *36*, L11201. https://doi.org/10.1029/2009GL038185

Zhou, X.-Z., Angelopoulos, V., Poppe, A. R., & Halekas, J. S. (2013). ARTEMIS observations of lunar pick-up ions: Mass-constraints on ion species. *Journal of Geophysical Research: Planets*, *118*, 1766–1774. https://doi.org/10.1002/jgre.20125

Zhou, X.-Z., Angelopoulos, V., Poppe, A. R., Halekas, J. S., Khurana, K. K., Kivelson, M. G., et al. (2014). Lunar dayside current in the terrestrial lobe: ARTEMIS observations. *Journal of Geophysical Research: Space Physics*, *119*, 3381–3391. https://doi.org/10.1002/2014JA019842